CrystEngComm

Accepted Manuscript

ROYAL SOCIETY OF CHEMISTRY

www.rsc.org/crystengcomm

CrystEngComm RSCPublishing

COMMUNICATION

Effect of ion beam assisted deposition on the growth of indium-tin-oxide (ITO) nanowires

Cite this: DOI: 10.1039/xoxxoooooox
Received
Accepted
DOI: 10.1039/xoxxoooooox
www.rsc.org/crystengcomm

Hak Ki Yu† and Jong-Lam Lee*

We developed a method to control the alignment and density of indium-tin-oxide (ITO) nanowires by using ion beam assisted deposition (IBAD). During electron beam evaporation, IBAD changed the randomly oriented branch type nanowires to aligned nanowires without branches. This is due to the energetic ion beams which play a role in nucleating tin containing indium nanodot at the initial stage of growth. The improved alignment of the ITO nanowires reduced the sensing time of ethanol gas.

Indium-tin-oxide (ITO: Sn doped In_2O_3) has been studied extensively in the optoelectronic industry because of its unique transparent and conducting properties.[1-3] Some of its disadvantages, such as the high cost of indium and the brittleness of the oxide itself, have been overcome by modern technologies (indium recycling and nanostructure fabrication).[4,5] Therefore, the ITO has remained as one of the most important transparent conducting materials. Moreover, the uniform ITO nanostructures provide a larger surface to volume ratio and higher crystallinity than a polycrystalline film, which are essential in producing highly efficient devices.

Typically the ITO nanowires can be produced by methods such as chemical vapor deposition,[6-8] pulsed laser deposition,[9] and electro-spinning,[10] etc. However, these growth methods use metal catalyst such as Au or self-catalyst (indium-tin) nanodot for the vapor-liquid-solid (VLS) process. In both cases, the substrate is heated to more than 800 °C to maintain the liquid Au phase and the carbo-thermal reaction (mixing In_2O_3 and SnO_2 powder with graphite powder to make pure indium-tin metal catalyst for VLS)[7,8] between graphite powder and In_2O_3 and SnO_2. Moreover, the by-products induced by Au and graphite, such as AuIn, $AuIn_2$, and metal carbonate, can degrade the quality of the ITO nano-structures.[11] Meanwhile, electron beam deposition based on self-catalyst VLS is most attractive method for growing ITO nanowires of the large area uniformity at low temperatures below 150 °C, where a conventional polymer material can tolerate.[5,11] Although electron beam deposition may be able to control the large area uniformity of ITO nanowires, it cannot easily control their density or alignment. Because the physics (light tracing, current flow, and gas dynamics in 3-dimensional nanostructures) of ITO nanowires applied devices strongly depends on the density and alignment of ITO nanowires, it is important to develop a method to control the growth of ITO nanowires during electron beam deposition. Meanwhile, ion beam assisted deposition (IBAD) has been widely used to control the orientation or density of a thin film.[12,13] If we apply IBAD to ITO nanowires growth, the high energy particle beam can modulate the heterogeneous nucleation of the catalyst for the VLS growth of ITO nanowires. In addition, the electrical force between the charged particle beam and the evaporated materials will affect the alignment of the nanowires.

In this work, we developed a method using IBAD to control the density and alignment of ITO nanowires grown by electron beam deposition. During the electron beam deposition, the energetic ion particles continuously collided with evaporated

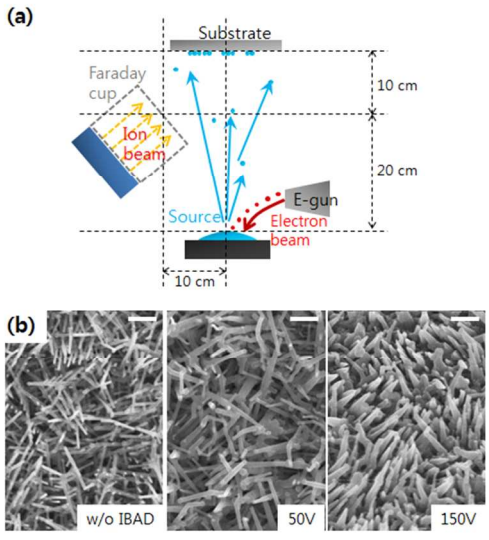

Fig. 1. (a) Schematic of IBAD system. (b) 45° tilted SEM images of ITO nanostructures with respect to ion beam intensity of 0 to 150 V. Beam current was set at 0.2 mA/cm^2. Scale bar, 200 nm.

Department of Materials Science and Engineering and Division of Advanced Materials Science, Pohang University of Science and Technology (POSTECH), Pohang, 790-784, Korea.
E-mail: jllee@postech.ac.kr; Fax: +82-54-279-5242;
Tel: +82-54-279-2152
†*Present Address: Max-Planck-Institut Für Biophysikalische Chemie, am Fassberg 11, 37077, Göttingen, Germany.*

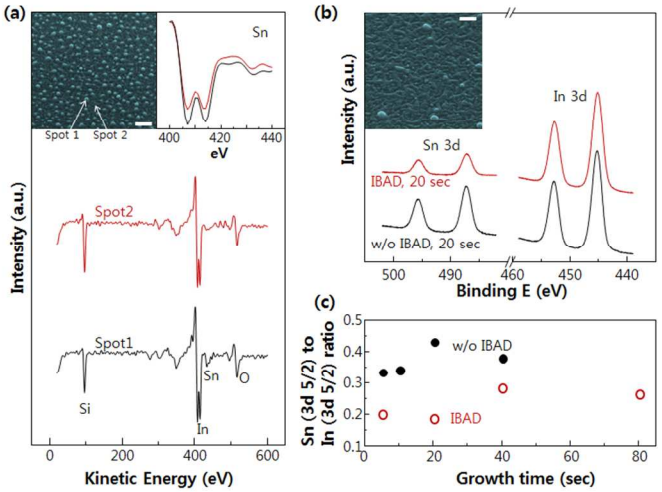

Fig. 2. (a) Auger spectra of spots 1 and 2 in inset SEM. The inset is a 45° tilted SEM image of the initial stage of ITO nanowires growth (for 20 s without IBAD). Scale bar, 100 nm. The enlarged graph is the Sn spectra of spots 1 and 2. (b) In and Sn *3d* XPS core level spectra of ITO nanowires grown for 20 s. The inset is a 45° tilted SEM image of the initial stage of ITO nanowires growth (during 20 s with IBAD). Scale bar, 100 nm. (c) Sn (*3d* 5/2) to In (*3d* 5/2) ratio of ITO nanowires with respect to growth time.

materials and adsorbed adatom, as shown in Fig. 1a, resulting in different types of ITO nanowires from the branch-type to the partially aligned-type. These ITO nanowires were applied as gas sensors and their chemisorption and desorption dynamics were compared, especially in terms of their response speed to ethanol vapor at room temperature.

An n-type (100) silicon substrate (doped with arsenic) covered by 150 nm thick thermal oxide was used as a starting substrate. The substrate was cleaned with acetone, ethyl alcohol, and deionized water. The ITO nanowires were fabricated using the electron beam deposition method. A tin doped (10 %) indium oxide pellet (purity: 99.99 %) was used as the source material. The ITO nanowires were grown at a rate of 0.5 nm s^{-1}. The chamber pressure was maintained at approximately 10^{-5} Torr during deposition and the substrate temperature was held at 300 °C to obtain well-developed ITO nanowires.[11] For IBAD, nitrogen (N_2) gas was inserted into the chamber, and the gas pressure was set to 0.2 mTorr. The ion beam voltage was modulated from 0 to 150 V, and the emission current was set to 0.2 mA/cm^2. Scanning electron microscopy (SEM) with PHILIPS XL30S was carried out at an acceleration voltage of 10 kV and working distance of 5 mm. Scanning Auger Microscopy (SAM) was carried out with ULVAC PHI700, VG 310F, which has 7 nm minimum beam size and 0.5 % element detection sensitivity. X-ray photoemission (XPS) was performed at the 4B1 beam line at Pohang Accelerator Laboratory (PAL). The incident photon energy of 630 eV was used to obtain In *3d* and Sn *3d* core level spectra. High-resolution X-ray diffraction (XRD) using synchrotron radiation was performed at the 3C2 beam line at PAL. High-resolution transmission electron microscopy (HRTEM) images were taken using a Cs-corrected JEM 2200FS operated at 200 kV. Gas sensor devices which adopted the ITO nanowires were fabricated, as described below. Soda-lime glass (2 cm × 2 cm) was used as the starting substrate. The glass was cleaned sequentially with acetone, ethyl-alcohol, and de-ionized water. After the growth of ITO nanowires on the substrate, Cr/Au (50 nm/200 nm) pad electrodes of 2 mm × 2 mm size were deposited on the nanostructures. The concentrations of ethanol gas of about 1000 ppm and 2000 ppm were calibrated by a conventional gas sensor, and gas of each concentration was injected by a mass flow controller onto the tops of the devices. The *I–V* changes according to the amount of gas adsorption/desorption were measured in ambient air at room temperature using a Keithley 2400 source measurement unit.

Figure 1b shows the 45° tilted-view SEM images of ITO nanowires grown for 300 s with respect to ion beam voltage intensity (emission current was set constant, 0.2 mA). The branch type ITO nanowires (synthesized under normal electron beam evaporation condition) gradually disappeared with the increase of ion beam voltage from 50 V to 150 V. To compare these morphological differences, we studied the early stage of ITO nanowire growth. The inset SEM image in Fig. 2a shows the ITO surface grown by normal electron beam deposition just for 20 s. Nano-size droplets were distributed for the VLS process. The detailed composition of the droplets was confirmed by Auger spectroscopy (Spot 1: droplet region, Spot 2: base region), as shown in Fig. 2a. The significant difference in Auger spectra is the tin concentration (Spot 1 has 43 % higher tin concentration than spot 2). The relatively high composition of tin promoted the formation of tin doped indium nano droplets due to the low melting point of the eutectic In(Sn) alloy (eutectic point of atomic concentration: 52 % indium and 48 % tin).[14] Moreover, the higher diffusivity of tin (~ 2.6×10^{-18} cm^2s^{-1}) than indium (~ 2.3×10^{-18} cm^2s^{-1}) in the In(Sn) alloy pro-

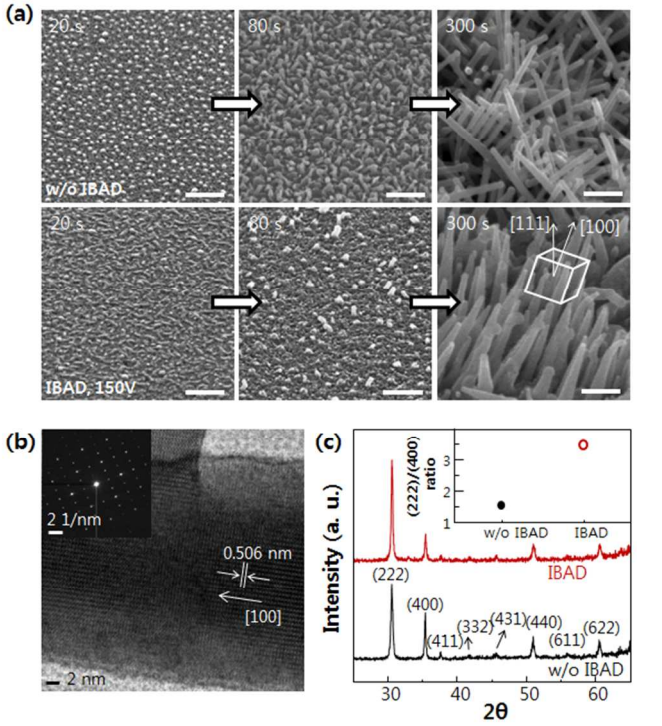

Fig. 3. (a) 45° tilted SEM images of ITO nanowires with respect to growth time from 20 s to 300 s. The schematic inset shows the (111) q_z diffraction of the (100) aligned cubic system. Scale bar, 100 nm. (b) High resolution TEM image and diffraction pattern of ITO nanowires grown by normal electron beam evaporation for 300 s. (c) X-ray

diffraction of ITO nanowires grown for 300 s. The inset is the intensity ratio of (222)/(400) peaks.

moted this phenomenon.[15] The effect of IBAD on the activity of tin during ITO evaporation could be checked by XPS measurement with respect to growth time. Figure 2b shows the In and Sn *3d* core level spectra for the ITO samples grown for 20 s with and without IBAD. The samples grown by IBAD showed about half the tin concentration of samples grown by the normal electron beam deposition method. This means that the IBAD can strongly reduce the density of In(Sn) nanodots for VLS growth, as shown in the inset SEM image of Fig. 2b. As shown in Fig. 2c (Sn *3d* to In *3d* ratio: these ratios were corrected by XPS sensitivity factor; Sn *3d* 5/2: 5.176 and In *3d* 5/2: 4.359),[16] this tendency is the same in the entire range of growth time from 5 s to 40 s. As the growth time increased, the ratio slightly decreased due to the development of ITO nanowires from In(Sn) nanodots.

Under the normal electron-beam evaporation condition, branch type ITO nanowires developed with time (Fig. 3a). The metallic In(Sn) nanodots, shown in the 20 second growth image, initiated the VLS process, resulting in ITO nanowires. ITO branches were developed by the additional nucleation of In(Sn) nanodots on the (100) family plane of the bixbyite ITO crystal.

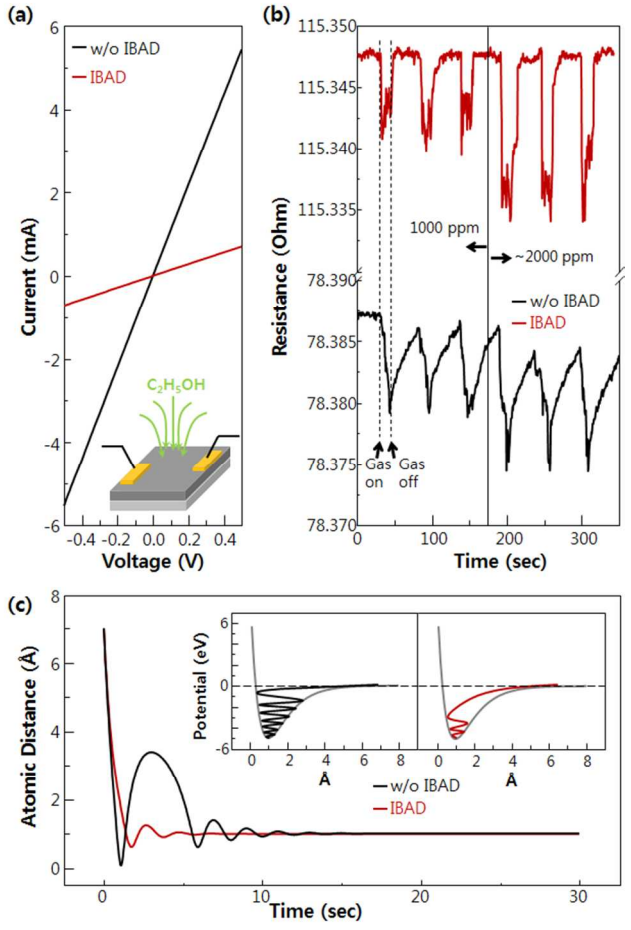

Fig. 4. The I-V curve for the Cr/Au contact pad on ITO nanowires. (b) Resistance changes of ITO nanowires with respect to repeated gas-on and gas-off operations and concentration. (c) Simulated trajectories of oxygen molecule for chemisorption on ITO nanowire surfaces following Morse potential. The inset is schematics of the trajectory motions on Morse potential curve.

However, the growth of ITO nanowires synthesized by IBAD (150 V, 0.2 mA condition) significantly differed, as shown in Fig. 3a. The nucleation of In(Sn) nanodots was suppressed by IBAD because the energetic ion beam blocked the migration of adatom, especially Sn. This blockage promoted the formation of nanodots through the reduction of the melting point of the eutectic type In(Sn) alloy. Moreover, the ion beam also blocked the additional nucleation of In(Sn) nanodots on the (100) family plane of ITO, resulting in nanowires without any branches, as shown in the 300 s growth image. The aligned ITO nanowires by IBAD could be understood as the result of electrical repulsion between individual nanowires during growth due to the formation of electrostatic force by IBAD.[17,18] The self-bias potential established on the immersed substrate surface in the ion plasma environment makes the electric field line of which is invariably terminated perpendicular to the surface.[18] The electrostatic force would force these one-dimensional nano-structures to align with the field direction, an energetically most favorable orientation. Because the (100) orientation of bixbyite ITO crystal is unstable due to the polarity, it has strong tendency to have reconstruction surface such as (111) facet,[19] resulting in tilt alignment from surface normal about 54.7° as shown in the inset of Fig. 3a. Each ITO nanowire was aligned in the bixbyite single crystal In_2O_3 (100) orientation with 0.506 nm spacing (Fig. 3b); this orientation was confirmed by a normal theta-2theta scan, as shown in Fig. 3c. The ITO nanowires formed by normal electron beam evaporation gave an XRD pattern with random orientation, showing all possible diffraction lines due to the randomly distributed (100) orientation of the branch structure. On the other hand, the ITO nanowires grown by IBAD showed a relatively strong (222) diffraction peak. This peak means that the ITO nanowires with (100) growth orientation were aligned in the (111) direction at 54.7° tilt angle.

We applied these ITO nanowires as gas sensors and compared their chemisorption and desorption dynamics, especially in terms of their response speed to ethanol vapor at room temperature, as shown in Fig. 4b. Basically, the initial resistance of the ITO nanobranches (~ 78 Ω) was lower than that of the IBAD ITO nanowires (~ 115 Ω) by about 32 % due to the many connections among the ITO nanowires (Fig. 4a). The mechanism responsible for the difference in resistance can be explained as follows. When the ITO nanowires were exposed to air, oxygen molecules chemisorbed onto the surface of the nanowires and captured electrons from the nanowires, making the nanowires less conductive. When the nanowires were exposed to a reducing gas such as ethanol vapor, the ethanol molecules reacted with the oxygen ions and released the electrons back into the conduction channel, thereby, reducing the resistance of the ITO nanowires.[20,21] There is a significant difference in the response time of the chemisorption-desorption process between the ITO nanobranches and the IBAD nanowires. The IBAD ITO nanowires showed a faster response time of about 1.5 ~ 2 s than the ITO nanobranches, which showed a response time of about 12 ~ 15 s. The resistance fluctuations of the IBAD ITO nanowires after exposure to ethanol were due to the interference of gas molecules between the reacted out-diffusion gas and the unreacted in-diffusion gas. Although ITO nanobranches also showed resistance fluctuations, the frequency of the fluctuations was significantly lower than that of the IBAD ITO nanowires due to the lower out-diffusion and in-diffusion

speeds of gas molecules through the dense branch structure. Similarly, the two devices showed different recovery times: 3 ~ 5 s for the IBAD ITO nanowires and ~ 40 s for the ITO nanobranches. There are two possible dynamic routes of oxygen molecule; one is physical scattering losing their energy as phonon of solid surfaces and the other is re-chemisorption and re-desorption loop in the nanostructure matrix. For the physical scattering route, the surface morphology of nanostructure is very important and the aligned nanorods by IBAD have merit for the fast translation of oxygen molecule than complex nanobranches shape. For the chemisorption-desorption loop route, we can focus on trajectories of gas molecule during chemisorption process based on Morse potential defined as $V(r)=D[1-exp\{-a(r-r_e)\}]^2-D$, where $V(r)$ is potential energy with respect to atomic distance r, D is potential depth at equilibrium bond distance r_e, and a is defined as $(k/2D)^{1/2}$ where k is spring constant.[22] In this potential curve, the first derivative is acceleration of gas molecule that approaches the specific surface. It is needed some friction to attach (chemisorption) gas molecule on specific solid surface, otherwise, the gas molecule will be easily scattered due to strong negative acceleration at the repulsion potential line (near close the surface). In this sense, the aligned ITO nanorods synthesized by IBAD could have larger friction coefficient than nanobranches because the friction coefficient strongly depends on the surface states such as point defect and depleted charge formed by energetic ion beam, resulting in fast chemisorption of oxygen molecules.[23] We can simply simulate the trajectories of oxygen gas molecule by assuming some variables in Morse potential; D is about 5 eV for the general chemisorption on oxide surface, r_e is about 1 Å, a is about 1 $Å^{-1}$.[24] If we assume the friction coefficient as 1.5 for IBAD ITO nanorods and 0.8 for ITO nanobranches, the trajectories of gas molecules could be calculated as shown in Fig. 4c. The oxygen molecule on ITO nanobranches shows multiple vibration path in the potential wall while that on IBAD ITO nanorods shows small number of vibration in the potential wall. So, the origin of fast response time in IBAD ITO nanorod could be understood as i) fast translation of gas molecule without multiple physical scattering in nanostructure matrix due to alignment and ii) fast chemisorption of oxygen gas due to large friction originated from defect at surface. We also have to think about the formation of nitride such as InN during IBAD. However there was no detection of nitride in crystallographic measurement such as XRD and TEM. Moreover, we also checked N *1s* spectra during XPS measurement, but, there was no nitrogen signal at all. Because the Gibbs free energy change for formation of In_2O_3 (-765.57 kJ/mole at 500K) is much lower than that of InN (-103.60 kJ/mole at 500K),[25] it is very difficult to happen that kind of nitride formation.

In this work, the effect of IBAD on the growth of ITO nanowires was studied. During electron beam evaporation, IBAD and its energetic ion beam changed the In(Sn) nanodot nucleation process and thus changed randomly oriented branch type nanowires to relatively well-aligned paralleled nanowires. The alignment of ITO nanowires significantly affected the response time of the ITO applied gas sensor, especially when ethanol gas was applied. This alignment and density control technique will be used to improve the performance of devices using ITO nanowires.

Acknowledgements
This work was supported in part by the Priority Research Centers Program through the National Research Foundation of Korea (NRF) funded by the Ministry of Education, Science and Technology (2010-0029711) and in part by the World Class University (WCU) program through the Korea Science and Engineering Foundation funded by the Ministry of Education, Science and Technology (Project No. R31-2008-000-10059-0).

References

1 Y. Park, V. Choong, Y. Gao, B. R. Hsieh and C. W. Tang, *Appl. Phys. Lett.*, 1996, **68**, 2699.
2 M. G. Mason, L. S. Hung, C. W. Tang, S. T. Lee, K. W. Wong and M. Wang, *J. Appl. Phys.*, 1999, **86**, 1688.
3 T. Margalith, O. Buchinsky, D. A. Cohen, A. C. Abare, M. Hansen, S. P. DenBaars and L. A. Coldren, *Appl. Phys. Lett.*, 1999, **74**, 3930.
4 S. –J. Hsieh, C. –C. Chen and W. C. Say, *Mater. Sci. Eng. B*, 2009, **158**, 82.
5 H. K. Yu, S. Kim, B. Koo, G. H. Jung, B. Lee, J. Ham and J. -L. Lee, *Nanoscale*, 2012, **4**, 6831.
6 Q. Wan, E. N. Dattoli, W. Y. Fung, W. Guo, Y. Chen, X. Pan and W. Lu, *Nano Lett.*, 2006, **6**, 2909.
7 X. Y. Xue, Y. J. Chen, Y. G. Liu, S. L. Shi, Y. G. Wang and T. H. Wang, *Appl. Phys. Lett.*, 2006, **88**, 201907.
8 A. J. Chiquito, A. J. C. Lanfredi and E. R. Leite, *J. Phys. D: Appl. Phys.*, 2008, **41**, 045106.
9 R. Savu and E. Joanni, *Scr. Mater.*, 2006, **55**, 979.
10 M. M. Munir, F. Iskandar, K. M. Yun, K. Okuyama and M. Abdullah, *Nanotechnology*, 2008, **19**, 145603.
11 H. K. Yu, W. J. Dong, G. H. Jung and J. –L. Lee, *ACS nano*, 2011, **5**, 8026.
12 C. P. Wang, K. B. Do, M. R. Beasley, T. H. Geballe and R. H. Hammond, *Appl. Phys. Lett.*, 1997, **71**, 2955.
13 L. Dong and D. J. Srolovitz, *Appl. Phys. Lett.*, 1999, **75**, 584.
14 H. Okamoto, *J. Phase Equilib. Diff.*, 2004, **27**, 313.
15 J. P. Daghfal and J. K. Shang, *J. Electron. Mater.*, 2007, **36**, 1372.
16 D. Briggs and M. P. Seah, Practical Surface Analysis by Auger and X-Ray Photoelectron Spectroscopy, Wiley, NewYork (1983).
17 W. Ahmed, E. S. Kooij, A. van Silfhout and B. Poelsema, *Nano Lett.*, 2009, **9**, 3786.
18 C. Bower, W. Zhu, S. Jin and O. Zhou, *Appl. Phys. Lett.*, 2000, **77**, 830.
19 E. H. Morales and U. Diebold, *Appl. Phys. Lett.*, 2009, **95**, 253105.
20 J. –H. Lee, *Sens. Actuators B*, 2009, **140**, 319.
21 N. Yamazoe, *Sens. Actuators B*, 2005, **108**, 2.
22 E. Shustorovich *Surf. Sci. Rep.*, 1986, **6**, 1.
23 W. Ahmed, E. S. Kooij, A. van Silfhout and B. Poelsema, *Nano Lett.*, 2009, **9**, 3786.
24 Y. D. Kim, A. P. Seitsonen, S. Wendt, J. Wang, C. Fan, K. Jacobi, H. Over and G. Ertl, *J. Phys. Chem. B*, 2001, **105**, 3752.
25 I. Barin, Thermochemical Data of Pure Substances, Wiley, New York (1989).

